Dalton Transactions

Accepted Manuscript

This is an *Accepted Manuscript*, which has been through the Royal Society of Chemistry peer review process and has been accepted for publication.

Accepted Manuscripts are published online shortly after acceptance, before technical editing, formatting and proof reading. Using this free service, authors can make their results available to the community, in citable form, before we publish the edited article. We will replace this *Accepted Manuscript* with the edited and formatted *Advance Article* as soon as it is available.

You can find more information about *Accepted Manuscripts* in the Information for Authors.

Please note that technical editing may introduce minor changes to the text and/or graphics, which may alter content. The journal's standard Terms & Conditions and the Ethical guidelines still apply. In no event shall the Royal Society of Chemistry be held responsible for any errors or omissions in this *Accepted Manuscript* or any consequences arising from the use of any information it contains.

ROYAL SOCIETY OF CHEMISTRY

www.rsc.org/dalton

Please do not adjust margins

Dalton Transactions

ARTICLE

One-pot Synthesis Polyamines Improved Magnetism and Fluorescence Fe_3O_4-Carbon Dots Hybrid NPs for Dual Modal Imaging

Received 00th January 20xx,
Accepted 00th January 20xx

DOI: 10.1039/x0xx00000x

www.rsc.org/

Bo Li,[a,b] Xudong Wang,[a] Yali Guo,[a] Anam Iqbal,[a] Yaping Dong,[b] Wu Li,[b] Weisheng Liu[a] ,Wenwu Qin[a*], Shizhen Chen[c], Xin Zhou[c], Yunhuang Yang[c*]

A one-step hydrothermal method was developed to fabricate Fe_3O_4-Carbon Dots (Fe_3O_4-CDs) magnetic–fluorescent hybrid nanoparticles (NPs). Ferric ammonium citrate (FAC) was used as cheap and nontoxic iron precursors and as for carbon source. And triethylenetetramine (TETA) was used as to improve the adhesive strength of CDs on Fe_3O_4 and fluorescence intensity of CDs. The prepared water-soluble hybrid NPs not only exhibit excellent superparamagnetic properties (Ms = 56.8 emu g^{-1}), but also demonstrate excitation-independent photoluminescent for down-conversion and up-conversion at 445 nm. Moreover, the prepared water-soluble Fe_3O_4-CDs hybrid NPs have a dual modal imaging ability for both magnetic resonance imaging (MRI) and fluorescent imaging.

1. Introduction

Integration of multiple discrete components to construct multifunctional NPs combined of different unique functionalities from all individual components has received more and more attention due to their potential applications in many fields.[1-4] In particular, functionalized superparamagnetic NPs with fluorescent performance have attracted significant interest for their excellent potential in a wide variety of biomedical applications such as magnetic resonance imaging (MRI), fluorescence imaging, drug delivery and photothermal therapy.[5-10] In order to construct magnetic–fluorescent hybrid NPs tremendous efforts have been developed to combine the magnetic and fluorescent materials into composite nano-functional materials with both of two properties of components simultaneously. For example Core/Shell and dumbbell-like structure magnetic–fluorescent hybrid NPs combined of noble metal NPs (Au or Ag NPs) or semiconducting quantum dots with superparamagnetic iron oxide have achieved and put up predominant performance in the field of biomedical applications.[11-14] However, there are some extent of limitations for conventional magnetic–fluorescent hybrid NPs for their preparation and use in many practical applications. For one thing these used fluorescent materials for instance organic dyes,[15, 16] SQDs,[13, 14] noble metal NPs,[11, 12] and rare earth metal NPs[17, 18] have more or less shortages such as poor photostability and biocompatibility, toxicity, and high cost. Furthermore, the complicated multi-step synthetic procedures for preparation of these magnetic–fluorescent composite NPs are another obstruction for their practical applications.

Recently a new type of fluorescence materials of CDs are widely considered to be advantageous over other fluorescent materials due to their outstanding optical properties, high photostability, good aqueous solubility, low toxicity, and excellent biocompatibility.[19-21] Based on these superior properties, CDs are more suitable for using in optical bioimaging as fluorescent agent for both in vitro and in vivo than the traditional fluorescent materials. For example, Sun et al.[22] reported that CDs surface passivated by PPEI-EI exhibit strong luminescence with two-photon excitation in the near-infrared and the results of two-photon luminescence microscopy imaging of the CDs internalized in human breast cancer cells indicated the potential of the CDs in cell imaging with two-photon luminescence microscopy. Yang et al.[23] studied CDs for optical imaging in vivo firstly in 2009. The surface passivated CDs and CDs@ZnS were injected into mice through subcutaneous, interdermal and intravenous injections and remained strongly fluorescent in vivo. In addition, CDs can be easily obtained via various synthetic methods from a wide range of low-cost and available raw materials.[24-27] Citric acid as one of the most potential precursor for synthesizing CDs through “bottom-up” method has been priority selected. Yang et al.[28] reported a facile and high output strategy for fabricating of CD with a quantum yield (QY) as high as ca. 80% by condensing CA and ethylenediamine to form polymer-like CDs and then carbonizing to form the CDs. And the relationship between chemical structure and PL mechanism were investigated in detail. Li et al.[29] produced nitrogen and sulfur co-

[a] Key Laboratory of Nonferrous Metal Chemistry and Resources Utilization of Gansu Province Lanzhou University, Lanzhou, 730000 (P.R. China) Fax: (+86) 931-8912582 E-mail: qinww@lzu.edu.cn.
[b] Qinghai Institute of Salt Lakes, Chinese Academy of Sciences, Xining, Qinghai 810008, (P.R. China)
[c] Key Laboratory of Magnetic Resonance in Biological Systems, State Key Laboratory of Magnetic Resonance and Atomic and Molecular Physics, National Center for Magnetic Resonance in Wuhan, Wuhan Institute of Physics and Mathematics, Chinese Academy of Sciences, Wuhan 430071, China. E-mail:yang_yh@wipm.ac.cn.
†Electronic supplementary information (ESI) available: See DOI: 10.1039/c5tb01938a.

Dalton Transactions Accepted Manuscript

doped CDs (N, S-CDs) using CA as carbon source and L-cysteine providing nitrogen and sulfur through a one-step hydrothermal treatment. The N, S-CDs exhibited very high QY (73%) and excitation-independent emission, resulting from the synergy effect of the doped nitrogen and sulfur atoms.

However, to the best of our knowledge there are only few hybrid NPs been reported combined magnetic nanocrystals with CDs for dual-modal imaging.[30] Carbon-dots possess magnetism have been reported by us before.[31] The preparation of magnetic–fluorescent hybrid NPs (Ni@SiO_2–CDs) required lengthy multi-step synthetic procedures. Thus, the purpose of this work is to present a simple one pot method to synthesize magnetic–fluorescent hybrid NPs. In our synthetic strategy ferric ammonium citrate (FAC) as a cheap and nontoxic iron precursor and the carbon source and triethylenetetramine (TETA) present in the reaction medium as reducing agent and nitrogen source, such that Fe (III) was reduced to form Fe_3O_4 NPs by TETA, meanwhile, citrate and TETA carbonized into nitrogen doped CDs. Finally hybrid NPs based on magnetic iron oxide and fluorescent CDs can be obtained in one-step conveniently. The obtained Fe_3O_4-CDs hybrid NPs not only show the superparamagnetic properties of the Fe_3O_4 nanocrystals for MRI contrast, but also manifest the compelling photoluminescent (PL) properties of the CDs, including excitation-independent emission and upconversion PL. The advantages of our preparation strategy in this study is eliminates the tedious preparation of magnetic–fluorescent hybrid NPs. In addition TETA is proved as major factor for the excellent properties of Fe_3O_4-CDs hybrid NPs by controlled trial. Therefore, these developed Fe_3O_4@ CDs hybrid NPs are non-toxic and low cost, which should be ideal candidates for combined dual-modal imaging diagnosis.

2. Experiment

2.1 Materials and instruments

Ferric ammonium citrate (FAC) and Triethylenetetramine (TETA, 70%) were purchased from Aladdin Reagent (Shanghai, China). Urea and citric acid monohydrate were purchased from Guangfu Reagent Company (Tianjin, China). Acetone was used as received without further purification. All reagents are Analytical Reagent grade. The water used in all experiments was deionized water prepared with Milli-Q water (18.2 MΩ cm).

XRD measurements were performed on a X-ray diffractometer (Philips X'Pert, Holland) with Cu Kα radiation (λ=1.54059Å), with operating voltage and current at 40 kV and 35 mA. X-ray photoelectron spectra (XPS) were acquired on a PHI 550 photoelectron spectrometer equipped with an Mg Kα (hv = 1253.6 eV). The X-ray gun operated at 15 kV and 20 mA. The background pressure of residual gases during the measurements was lower than 10^{-6} Pa. The transmission electron microscopy (TEM) was taken on a JEM-2100 transmission electron microscope at an acceleration voltage of 120 kV. Dynamic light scattered (DLS) was got on a BI-200SM (USA Brookhaven) at room temperature. Fourier transform infrared (FTIR) spectra were measured using a Nicolet 360 FTIR spectrometer with the KBr pellet technique. The magnetic behavior was tested using a vibrating sample magnetometer (VSM, Lake Shore 7304, Lake Shore, USA) at room temperature. UV–vis absorption spectra were obtained on an Agilent UV Cary100 spectrophotometer. FLS920 spectrofluorometer was used to measure steady-state emission spectra, fluorescence lifetimes and quantum yields. Quantum yields were determined by a relative method using quinine sulfate as fluorescence standard. Fluorescence imaging was performed on an Olympus FV1000-IX81 laser confocal microscope. T_2-weighted MR images were performed on a 7.0 T MRI scanner (Bruker BioSpec 70/20 USR), R_2 values were measured on a Bruker 500 MHz NMR spectrometer.

2.2 Preparation of Fe_3O_4-CDs hybrid NPs

In a typical synthesis, AFC (0.133 g) was dissolved in H_2O and TETA 10 mL (volume ratio 9:1). The precursor solution was transferred to a 20 ml Teflon-lined stainless steel autoclave. After sealing, the autoclave was heated to and maintained at 200 °C for 2, 4 and 6 h. The autoclave was then cooled naturally to room temperature. The soliquoid was separated by centrifugation (6500 r min^{-1}, 2 min) to discard liquid phase. The obtained solid phase was dispersed in 10 ml acetone by ultrasonic dispersing for 3 minutes then magnetic separating. This washing process repeated for three times to remove dissociative CDs and TETA. Finally, the black products were dried in air-circulating oven at 60°C. By contrast, the synthesis without TETA was also performed. The samples are thereafter denoted as Fe_3O_4-CDs and Fe_3O_4, respectively.

2.3 In vitro MRI studies

Magnetic resonance imaging (MRI) tests were performed on a 7.0 T MRI scanner (Bruker BioSpec 70/20 USR). Fe_3O_4-CDs NPs were dispersed in deionized water with various concentrations and then taken 200 μL into 96-well plate. The T_2-weighted images were acquired using multi-slice-multi-echo sequence (MSME) with the following parameters: echo time = 100 ms, repetition time = 2000 ms, field of view = 2 ×2 cm^2, number of average = 1, matrix size = 128 × 96 (data zero filled to a 256 x 256 matrix).

R_2 values of Fe_3O_4-CDs NPs were measured using the Carr-Purcell-Meiboom- Gill (CPMG) sequence with a bradband decoupling inverse 1H probe (BBI) on the Bruker 500 MHz NMR spectrometer. Fe_3O_4-CDs NPs were dispersed in 98 % deuterium oxide with various concentrations and then taken 500 μL into 5 mm sample tubes.

2.4 Cell culture, fluorescence imaging and cytotoxicity assay

Cellular fluorescent images were recorded using an Olympus FV1000-IX81 laser confocal microscope. BHK cells were cultured in DMEM (Dulbecco's Modified Eagle Medium) supplemented with 10% FBS (fetal bovine serum). The cell lines were maintained under a humidified atmosphere containing 5% CO_2 at 37 °C. After the removal of the culture medium, cells were incubated with 200 μgml^{-1} Fe_3O_4-CDs hybrid NPs in 1.0 ml of fresh culture medium for 2 h. The cells were washed three times with PBS to remove the residual nanoparticles before the imaging measurement.

Cytotoxicity Test. BHK Cells were seeded at a density of 10^4 cells per well (100 μL total volume/well) in 96-well assay plates for 24 h. Then, the as-prepared Fe_3O_4-CDs hybrid NPs were added to the cell culture medium at the indicated concentrations (20, 40, 80, 160, 200 μgmL^{-1}). Cells were incubated with Fe_3O_4-CDs for 24 h. To determine toxicity, 3-(4,5-Dimethylthiazol-2-yl)-5-(3-

Dalton Transactions Accepted Manuscript

 This journal is © The Royal Society of Chemistry 20xx

carboxymethoxyphenyl)-2-(4-sulfophenyl)-2H-tetrazolium, inner salts (MTS) was added to each well of the microtiter plate and the plate was incubated in the CO_2 incubator for additional 4 h. Absorbance values were determined with Bio-Rad model-680 microplate reader at 490 nm (corrected for background absorbance at 630 nm). The cell viability was estimated according to the following equation: cell viability (%) = mean of absorbance value of treatment group/mean absorbance value of control × 100%.

3. Results and discussion

The Fe_3O_4-CDs hybrid NPs were synthesized by one-step hydrothermal method. The obtained Fe_3O_4-CDs hybrid NPs exhibits good water solubility and shows bright blue luminescence under excitation of a 365 nm UV lamp in water. But the product synthesized without TETA have no luminescence under the same condition, which is due to that CDs produced during synthesis process was washed away by acetone from the surface of Fe_3O_4

3.1 Physical structure of Fe_3O_4-CDs

Fig. 1 gives the results of XRD analysis of obtained nano-particles under different hydrothermal time and solution environment. The reflections of 111, 220, 311, 400, 422, 511 and 440 in the typical XRD pattern can be matched well with the standard magnetic Fe_3O_4 according to JCPDS card No. 19-0629. Obviously, the degree of crystalline of the samples synthesized with TETA (a, b, c) is better than those synthesized without TETA (d, e, f) and increase with the hydrothermal time turns longer. The result demonstrates that TETA and longer hydrothermal time are beneficial to produce well-crystallized Fe_3O_4 nanoparticles by hydrothermal technique. This kind of improvement of hydrophilic TETA in the synthesis of iron oxide NPs is observed in the previous study.[32] It believes that TETA provide a reductive environment to reduce the iron precursors partially and facilitate the nucleation and subsequent growth period. The reason for no typical reflection of CDs in 20-25° detected for Fe_3O_4-CDs hybrid NPs may be because of relatively low content and poor crystallinity of CDs in Fe_3O_4-CDs hybrid NPs. The XRD pattern of TETA-CDs obtained by hydrothermal time 6 h at 200 °C is given in Fig. S1 and a broad diffraction peak centered at 2θ = 23° (d_{002} = 0.31 nm) is detected as other reports.[29, 33]

Fig. 2 shows the typical transmission electron microscopy (TEM) images of Fe_3O_4 and Fe_3O_4-CDs hybrid NPs with hydrothermal time 6 h. The TEM image (Fig. 2 A) shows that Fe_3O_4 NPs appear irregular in morphology and size ranging from several nanometers to tens of nanometers. In contrast, the Fe_3O_4-CDs hybrid NPs (Fig. 2B) posses rather uniform particle morphology and size. The result of dynamic light scattering (DLS) measurement (inset of Fig. 2B) shows that the size of Fe_3O_4-CDs hybrid NPs are distributed in the range from 9 to 13 nm, with an average size of 12 nm. These results including with XRD analysis indicate that TETA plays a critical role in modifying the particle and crystallite characteristics. High-resolution TEM (HRTEM) image (Fig. 2C) reveals the high crystallinity of the Fe_3O_4-CDs hybrid NPs. The lattice spacing of 0.32 nm should be the spacing between graphene layers (002 facet) which is similar to that of many other reported CDs.[29, 34-36] The interplanar spacing about 0.25 nm and 0.29 nm corresponding to the (3 1 1) and (2 2 0) lattice plane of the cubic Fe_3O_4 (0.253 nm and 0.297 nm) respectively. To further confirm the formation of the composite structure, energy dispersive

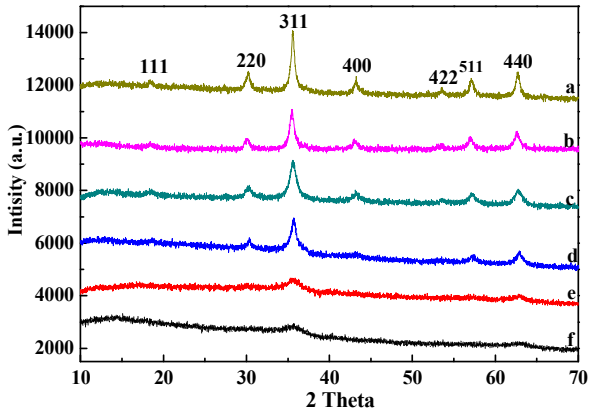

Fig. 1 XRD patterns of Fe_3O_4 -CDs and Fe_3O_4: a, b, c are Fe_3O_4 -CDs with hydrothermal time 6 h, 4 h, 2 h and d, e, f are Fe_3O_4 with hydrothermal time 6 h, 4 h, 2h.

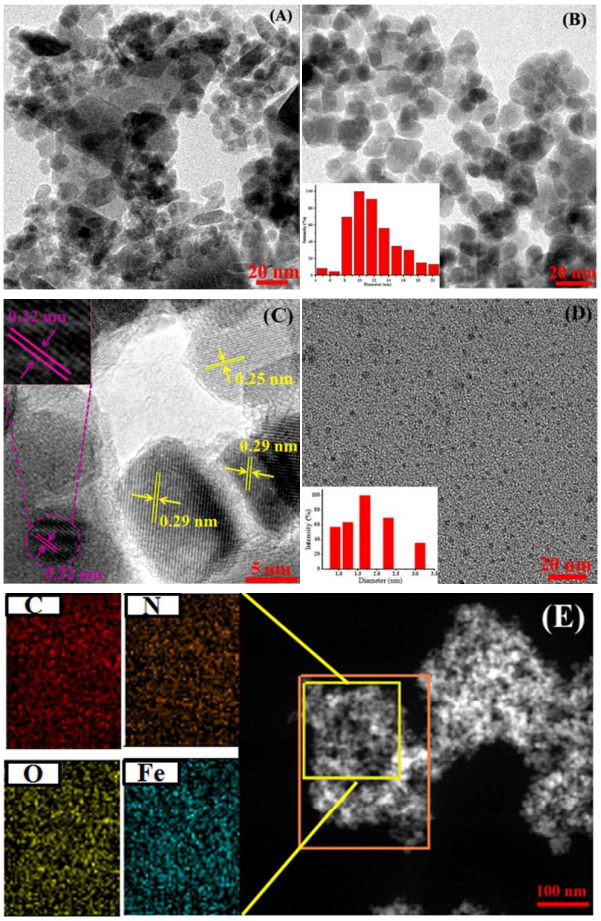

Fig. 2 TEM images of Fe_3O_4 (A), Fe_3O_4-CDs and size distribution histogram (inset) (B), HRTEM image of Fe_3O_4-CDs and enlarged selection area (inset) (C), TEM image of as-prepared TETA-CDs hydrothermal time 6 h at 200 °C and size distribution histogram (inset) (D) and EDS element mapping data of Fe, O, C and N elements throughout the Fe_3O_4-CDs (E).

Dalton Transactions Accepted Manuscript

X-ray spectroscopy (EDS) element mapping is recorded and shown in Fig. 2E. (EDS) element mapping clearly shows the elements of Fe, O, C and N evenly distributed in Fe_3O_4-CDs hybrid NPs. It is shown that the CDs have good dispersivity with Fe_3O_4 particles from the (EDS) element mapping results. The morphology of TETA-CDs are also characterized by TEM and dynamic light scattering (DLS) measurements as shown in Fig. 2D. The size of the as prepared TETA-CDs is distributed in the range from 1 to 3 nm, with an average size of 2 nm.

3.2 Chemical structure of Fe_3O_4-CDs

The X-ray photoelectron spectra (XPS) were employed to investigate the surface composition of as prepared Fe_3O_4-CDs and Fe_3O_4 NPs. Fig. 3A presents the XPS full-scan spectra of Fe_3O_4-CDs and Fe_3O_4 NPs. Obviously, the XPS spectra indicate that both Fe_3O_4-CDs and Fe_3O_4 NPs are composed of ferrum, oxygen and carbon. However, nitrogen is detected only in Fe_3O_4-CDs hybrid NPs. The high-resolution spectra of C1s of Fe_3O_4-CDs hybrid NPs (Fig. 3B) can be de-convoluted into three peaks at 284.6, 286.2, and 288.0 eV assigning to carbon in the form of C-C, C=N and C=O respectively.[29, 37] The N 1s high-resolution spectra (Fig. 3C) displays two peaks at399.2 and 400.6 indicating that nitrogen exists mostly in the form of pyridinic-like N and pyrrolic-like N.[37]

To further confirm the chemical composition of Fe_3O_4-CDs, FT-IR spectra were recorded to identify the functional groups. As given in Fig. 3D, the main bands of Fe_3O_4 NPs at 3389 cm^{-1}, 1626 cm^{-1}, 1400 cm^{-1} are for the O-H stretching vibration, C=O stretching vibration, C-O bending vibration and the bands of 581 cm^{-1} and 443 cm^{-1} are attribute to Fe-O bond.[38] The intense band at 1626 cm^{-1} for Fe_3O_4 NPs reveals the binding of a CA radical to surface of Fe_3O_4 NPs. CA as coordinating ligand could stabilize the Fe_3O_4 NPs to some extent but would not influence the magnetic and hardly immobilize CDs on the surface of Fe_3O_4 NPs. Corresponding to Fe_3O_4-CDs, the band at 3393 cm^{-1} indicate the existence of O-H and N-H. The broader band at 1561 cm^{-1} with a shoulder about 1637 cm^{-1} may be due to N-H bending vibration and amide I C=O stretching vibration.[39] The weak band at 1310 cm^{-1} is assigned to C-N

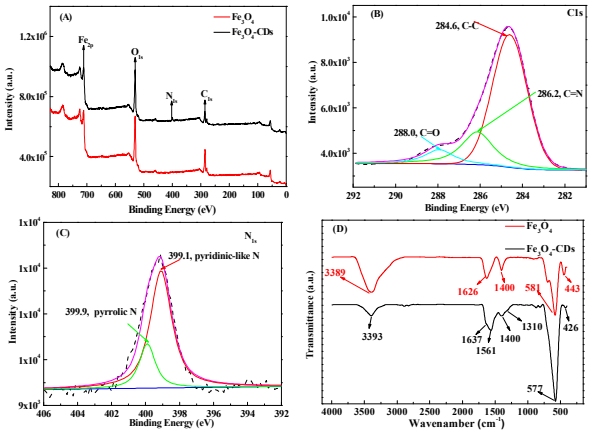

Fig. 3 XPS full-scan spectra of Fe_3O_4 and Fe_3O_4-CDs NPs (A), XPS high resolution survey scan of (B) C1s, and (C) N1s region of Fe_3O_4-CDs NPs, (D) FT-IR spectra of Fe_3O_4 and Fe_3O_4-CDs NPs.

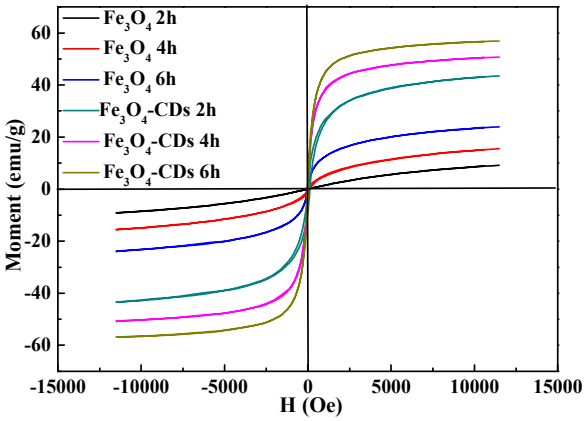

Fig. 4 Room-temperature magnetization curves of Fe_3O_4-CDs and Fe_3O_4 with different hydrothermal time.

stretching vibration. The bands at 1400 cm^{-1}, 577 cm^{-1} and 426 cm^{-1} refer to C-O, Fe-O bonds respectively like as Fe_3O_4. Both XPS and FT-IR spectra results indicate that N doped CDs was synthesized with TETA and attached on the surface of Fe_3O_4 nanoparticles.

3.3 Magnetic and Optical Properties of Fe_3O_4-CDs

The magnetic properties of Fe_3O_4-CDs and Fe_3O_4 NPs were measured at room temperature with a vibrating sample magnetometer (VSM). Fig. 4 shows the magnetization of magnetite nanocrystals prepared under different solution conditions and hydrothermal time. The saturation magnetizations of Fe_3O_4-CDs with hydrothermal time 2 h, 4 h, 6 h are 43.2, 50.6, 56.8 emu/g respectively which are much higher than the best one of Fe_3O_4 23.7 emu/g with 6 h hydrothermal time. The saturation magnetization of Fe_3O_4-CDs do not decrease than no hybridized Fe_3O_4, which is not like the previous magnetic composite materials.[31, 40] The great gap of saturation magnetization between Fe_3O_4-CDs and Fe_3O_4 should be mainly attributed to the better crystallinity benefited from the improvement of TETA as shown in Fig. 1. And the longer hydrothermal time also effectively promoted the magnetism of Fe_3O_4-CDs and Fe_3O_4 by increasing crystallinity as well.

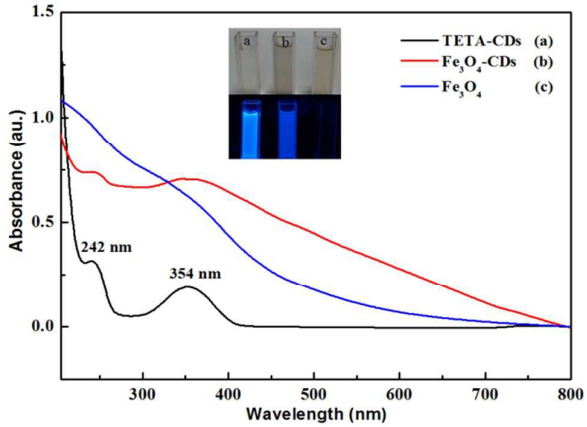

Fig. 5 UV-vis absorption spectra of TETA-CDs, Fe_3O_4-CDs and Fe_3O_4 in water. The inset is the samples under day light and UV lamp (the excitation wavelength is 365 nm).

Dalton Transactions Accepted Manuscript

This journal is © The Royal Society of Chemistry 20xx

Fig. 5 shows UV-vis absorption spectra of TETA-CDs, Fe_3O_4-CDs and Fe_3O_4 in aqueous solution, the inset is corresponding photographs taken under daylight and UV lamp. TETA-CDs shows two typical absorption peaks at 242 and 354 nm. The peak at 242 nm ascribes to the π-π* transition of C=C band and the other peak at about 354 nm derives from the trapping of excited state energy by the surface states leading to strong FL signal.[29] The absorption of Fe_3O_4-CDs also shows two obvious absorption peaks at the same wavelength, while the absorption of Fe_3O_4 has no obvious absorption peaks in the UV-vis light area. This result indicates that CDs keep good photoresponse in UV-vis light area like TETA-CDs unaffected by iron ion in the synthetic process. In addition, introducing TETA effectively improves the adhesion of Fe_3O_4 and CDs due to presence of amine on the surface of CDs. The UV-vis absorption spectra of CA-CDs and N-CDs in aqueous solution as shown in Fig. S2. N-CDs have two absorption peaks at 235 and 335 nm which are blue-shifted relative to the corresponding absorption peaks of TETA-CDs. While, CA-CDs have no obvious absorption peaks in UV-vis light area.

The photoluminescent properties of Fe_3O_4-CDs were examined in water at different excitation wavelengths as shown in Fig. 6A. Unlike most CDs, the emission wavelength of the Fe_3O_4-CDs at 445 nm and hardly shift as the excitation wavelength changed from 300 nm to 410 nm. The maximum excitation wavelength of the Fe_3O_4-CDs aqueous solution is 360 nm. The emission wavelength of TETA-CDs is also excitation independent with maximum excitation wavelength and fixed emission wavelength 370 nm and 445 nm respectively as illustrated in Fig. S 3A. This result indicates that CDs in Fe_3O_4-CDs hybrid NPs may have the same mechanism of luminescence as TETA-CDs. But the FL quantum yield (FLQY) of Fe_3O_4-CDs decrease dramatically by contrast with TETA-CDs. The FL quantum yield of TETA-CDs is about 53% excited with 360 nm light, while the FL quantum yield of Fe_3O_4-CDs is only about 4.6%. The acute quenching of the Fe_3O_4-CDs is due to static and dynamic fluorescence quenching of the dots and strong absorption of the transmitted light by the iron oxide particles as showed in Fig. 5.[41]

The up-conversion PL properties of Fe_3O_4-CDs and TETA-CDs were also investigated as shown in Fig. 6B and Fig. S 3B. The up-conversion PL spectra also shows a fixed emission peak at the same wavelength of 445 nm as down-conversion PL spectra and remained unchanged when the excitation wavelength varies, which indicated that the emission occurs from the lowest single state regardless of the mode of excitation like as observing in microwave-assisted synthesized DEG-CDs.[33] However, the photoluminescent properties of CA-CDs and N-CDs are different from Fe_3O_4-CDs and TETA-CDs. The emission wavelengths of CA-CDs and N-CDs are excitation dependent including down-conversion and up-conversion as shown in Fig. S4 and Fig. S5. These results imply that TETA not only acts as nitrogen source for CDs synthesis with CA but also helps to form a relatively uniform surface status.[29]

To investigate the fluorescence dynamics of Fe_3O_4-CDs and TETA-CDs, fluorescence decay traces of Fe_3O_4-CDs and TETA-CDs were recorded at three emission wavelengths (440 nm, 460 nm and 480 nm) by the single-photon timing method. The fluorescence

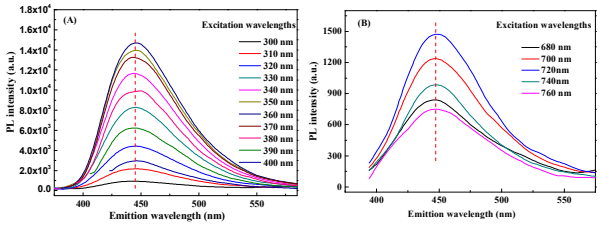

Fig. 6 Fluorescence spectra of the Fe_3O_4-CDs different excitation wavelengths: (A) down-conversion and (B) up-conversion.

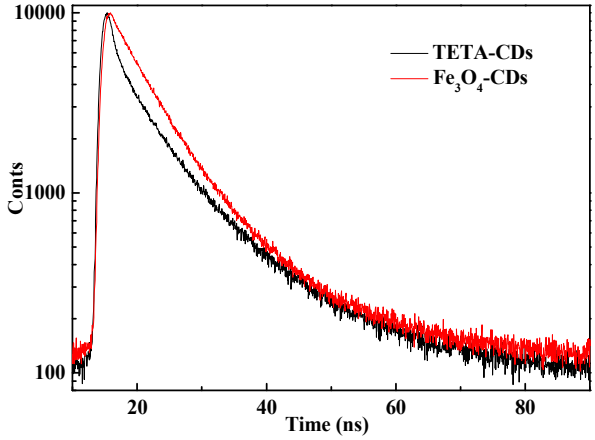

Fig. 7 The decay curves of Fe_3O_4-CDs and TETA-CDs in aqueous solution collected at 440 nm when excited at 360 nm.

decays for the Fe_3O_4-CDs and TETA-CDs aqueous solution were studied as shown in Fig. 7 and Table S1.

The fluorescence decay of TETA-CDs aqueous solution at λ_{ex}= 360 nm can be described as tri-exponential function with the contributions of the τ_1 (~14 ns, 39%), τ_2 (~ 5 ns, 46%) and τ_3 (~0.8 ns, 15%). The multiexponential nature of the lifetime suggests that the components of TETA-CDs in water are complicated, probably due to the involvement of different particle sizes and emissive trap sites. While, the fluorescence decay of Fe_3O_4-CDs aqueous solution described as bi-exponential function with the contributions of the τ_1 (~ 13 ns, 34%) and τ_2 (~ 5 ns, 66%) at the same excitation wavelength λ_{ex}= 360 nm. The presence of Fe_3O_4 in the TETA-CDs does not change the two longer fluorescence lifetimes (~ 14 ns and ~5 ns) of TETA-CDs.

3.4 In vitro MRI

In order to evaluate the T_2 contrast properties of the Fe_3O_4-CDs NPs, the T_2-weighted images of the as-prepared NPs dispersed in deionized water with different concentrations (I, 2 μg/mL; II, 4 μg/mL; III, 6 μg/mL; IV, 8 μg/mL; V, 16 μg/mL; VI, 32 μg/mL; VII, 48 μg/mL) were obtained in a Bruker Biospec 7.0 T MRI system at room temperature. It can be clearly seen that the signal intensity of the MR images is related to the concentration of Fe_3O_4-CDs NPs (Fig. 8). The r_2 value of the Fe_3O_4-CDs NPs was r_2 = 0.02588 $mL*\mu g^{-1}*s^{-1}$ measured in a Bruker 500 MHz NMR spectrometer (Fig. 9). Those results indicate that the as-prepared Fe_3O_4-CDs NPs could be used as a T_2 contrast agent in MRI.

Dalton Transactions Accepted Manuscript

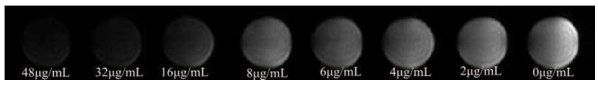

Fig. 8 T_2-weighted MR images of Fe_3O_4-CDs at various concentrations at 7 T.

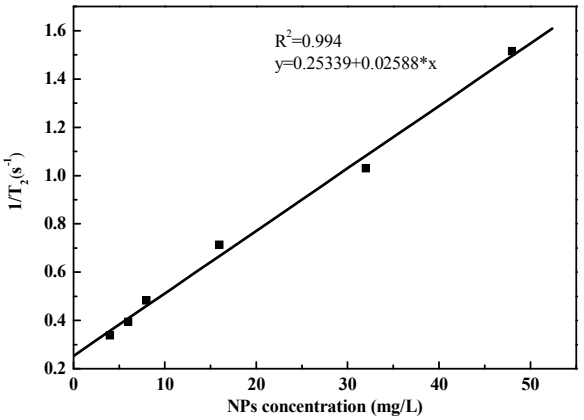

Fig. 9 Plot of R_2 values of the Fe3O4-CDs NPs.

3.5 Cell imaging

It is expected that the Fe_3O_4-CDs hybrid NPs should have a dualmodal imaging ability for both MRI and fluorescent imaging. For living cell labeling and imaging, the bioimaging properties of Fe_3O_4-CDs using a confocal microscope with BHK cells was performed. BHK cells loaded with Fe_3O_4-CDs for 2 h at 37 °C shows bright blue luminescence excited with 365 nm UV light as shown in Fig. 10. The laser scanning confocal images clearly indicate that can transfer into the living cells. The results suggest that Fe_3O_4-CDs have great application potential in multimodal bioimaging with the fluorescent imaging ability of the CDs and superparamagnetism ability of the Fe_3O_4. In addition, cell cytotoxicity experiments of Fe_3O_4-CDs hybrid NPs were evaluated using BHK cell lines through the MTS assay. As shown in Fig. S7, the Fe_3O_4-CDs exhibited low cytotoxicity, which may be due to the low toxicity of CDs.

4. Conclusions

In summary, magnetic–fluorescent hybrid NPs Fe_3O_4 -CDs has been synthesized from a precursor ferric ammonium citrate and triethylenetetramine through a simple one-pot hydrothermal route. The advantages of our preparation strategy are this synthesis eliminates the tedious preparation of magnetic–fluorescent hybrid NPs. The excellent superparamagnetic and excitation-independent emission properties in water of Fe_3O_4-CDs hybrid NPs make them have great application potential in multimodal bioimaging. In addition, triethylenetetramine is proved as major factor for the excellent properties of Fe_3O_4-CDs hybrid NPs and excitation-independent emission properties of CDs by controlled trial.

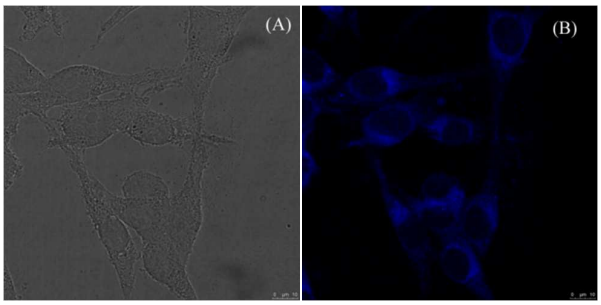

Fig. 10 Fluorescence image of BHK cells incubated with 200 μg ml^{-1} of Fe_3O_4 -CDs. The bright-field images (A) and the confocal fluorescence images (B).

Acknowledgements

This work was supported by the National Science Foundation for Fostering Talents in Basic Research of the National Natural Science Foundation of China (Grant no. J1103307). The authors would like to thank the Natural Science Foundation of China (no. 21271094, 21305156). Y Yang would like to thank the Hundred Talent Program by Chinese Academy of Sciences.

Notes and references

1 E. Roy, S. Patra, D. Kumar, R. Madhuri and P. K. Sharma, *Biosens. Bioelectron.*, 2015, **68**, 726-735.
2 X. L. Qiu, Q. L. Li, Y. Zhou, X. Y. Jin, A. D. Qi and Y. W. Yang, *Chem. Commun.* 2015, **51**, 4237-4240.
3 L. Huang, L. Ao, W. Wang, D. Hu, Z. Sheng and W. Su, *Chem. Commun.* 2015, **51**, 3923-3926.
4 Y. Chen, K. Ai, J. Liu, G. Sun, Q. Yin and L. Lu, *Biomaterials*, 2015, **60**, 111-120.
5 C. Tudisco, M. T. Cambria, F. Sinatra, F. Bertani, A. Alba, A. E. Giuffrida, S. Saccone, E. Fantechi, C. Innocenti, C. Sangregorio, E. Dalcanale and G. G. Condorelli, *J. Mater. Chem. B*, 2015, **3**, 4134-4145.
6 J. Shen, Y. Li, Y. Zhu, X. Yang, X. Yao, J. Li, G. Huang and C. Li, *J. Mater. Chem. B*, 2015, **3**, 2873-2882.
7 K. Yang, L. Hu, X. Ma, S. Ye, L. Cheng, X. Shi, C. Li, Y. Li and Z. Liu, *Adv. Mater.*, 2012, **24**, 1868-1872.
8 Z. Fan, M. Shelton, A. K. Singh, D. Senapati, S. A. Khan and P. C. Ray, *ACS nano*, 2012, **6**, 1065-1073.
9 L. Cheng, K. Yang, Y. Li, X. Zeng, M. Shao, S.-T. Lee and Z. Liu, *Biomaterials*, 2012, **33**, 2215-2222.
10 L. Cheng, K. Yang, Y. Li, J. Chen, C. Wang, M. Shao, S. T. Lee and Z. Liu, *Angew. Chem.*, 2011, **123**, 7523-7528.
11 J. Jiang, H. Gu, H. Shao, E. Devlin, G. C. Papaefthymiou and J. Y. Ying, *Adv. Mater.*, 2008, **20**, 4403-4407.
12 Z. Xu, Y. Hou and S. Sun, *J. Am. Cheml. Soc.*, 2007, **129**, 8698-8699.
13 S. Selvan, P. K. Patra, C. Y. Ang and J. Y. Ying, *Angew. Chem.*, 2007, **119**, 2500-2504.
14 H. Gu, R. Zheng, X. Zhang and B. Xu, *J. Am. Cheml. Soc.*, 2004, **126**, 5664-5665.
15 S. K. Yen, D. Janczewski, J. L. Lakshmi, S. B. Dolmanan, S. Tripathy, V. H. Ho, V. Vijayaragavan, A. Hariharan, P. Padmanabhan and K. K. Bhakoo, *ACS nano*, 2013, **7**, 6796-6805.
16 J. E. Lee, N. Lee, H. Kim, J. Kim, S. H. Choi, J. H. Kim, T. Kim, I. C. Song, S. P. Park and W. K. Moon, *J. Am. Cheml. Soc.*, 2009, **132**, 552-557.
17 H. Zhu, J. Tao, W. Wang, Y. Zhou, P. Li, Z. Li, K. Yan, S. Wu, K. W. Yeung and Z. Xu, *Biomaterials*, 2013, **34**, 2296-2306.

Dalton Transactions Accepted Manuscript

This journal is © The Royal Society of Chemistry 20xx

Please do not adjust margins

18 H. Zhu, Y. Shang, W. Wang, Y. Zhou, P. Li, K. Yan, S. Wu, K. W. Yeung, Z. Xu and H. Xu, *Small*, 2013, **9**, 2991-3000.
19 X. T. Zheng, A. Ananthanarayanan, K. Q. Luo and P. Chen, *Small*, 2015, **11**, 1620-1636.
20 S. Ray, A. Saha, N. R. Jana and R. Sarkar, *The J. Phys. Chem. C*, 2009, **113**, 18546-18551.
21 Y.-P. Sun, B. Zhou, Y. Lin, W. Wang, K. S. Fernando, P. Pathak, M. J. Meziani, B. A. Harruff, X. Wang and H. Wang, *J. Am. Cheml. Soc.*, 2006, **128**, 7756-7757.
22 L. Cao, X. Wang, M. J. Meziani, F. Lu, H. Wang, P. G. Luo, Y. Lin, B. A. Harruff, L. M. Veca and D. Murray, *J. Am. Cheml. Soc.*, 2007, **129**, 11318-11319.
23 S.-T. Yang, L. Cao, P. G. Luo, F. Lu, X. Wang, H. Wang, M. J. Meziani, Y. Liu, G. Qi and Y.-P. Sun, *J. Am. Cheml. Soc.*, 2009, **131**, 11308-11309.
24 S. Sahu, B. Behera, T. K. Maiti and S. Mohapatra, *Chem. Commun.*, 2012, **48**, 8835-8837.
25 X. Wang, K. Qu, B. Xu, J. Ren and X. Qu, *J. Mater. Chem.*, 2011, **21**, 2445-2450.
26 Q. Wang, H. Zheng, Y. Long, L. Zhang, M. Gao and W. Bai, *Carbon*, 2011, **49**, 3134-3140.
27 F. Wang, S. Pang, L. Wang, Q. Li, M. Kreiter and C.-y. Liu, *Chem. Mater.*, 2010, **22**, 4528-4530.
28 S. Zhu, Q. Meng, L. Wang, J. Zhang, Y. Song, H. Jin, K. Zhang, H. Sun, H. Wang and B. Yang, *Angew. Chem.*, 2013, **125**, 4045-4049.
29 Y. Dong, H. Pang, H. B. Yang, C. Guo, J. Shao, Y. Chi, C. M. Li and T. Yu, *Angew. Chem.*, 2013, **52**, 7800-7804.
30 Z. Markova, A. B. Bourlinos, K. Safarova, K. Polakova, J. Tucek, I. Medrik, K. Siskova, J. Petr, M. Krysmann, E. P. Giannelis and R. Zboril, *J. Mater. Chem.*, 2012, **22**, 16219-23.
31 D. Wang, Y. Guo, W. Liu and W. Qin, *RSC Adv.*, 2014, **4**, 7435-9.
32 H. Qu, H. Ma, A. Riviere, W. Zhou and C. J. O'Connor, *J. Mater. Chem.*, 2012, **22**, 3311-3.
33 Y. Liu, N. Xiao, N. Gong, H. Wang, X. Shi, W. Gu and L. Ye, *Carbon*, 2014, **68**, 258-264.
34 Y. Xu, M. Wu, Y. Liu, X. Z. Feng, X. B. Yin, X. W. He and Y. K. Zhang, *Chem. Eur. J.*, 2013, **19**, 2276-2283.
35 Z. C. Yang, M. Wang, A. M. Yong, S. Y. Wong, X. H. Zhang, H. Tan, A. Y. Chang, X. Li and J. Wang, *Chem. Commun.* 2011, **47**, 11615-11617.
36 H. Ding, J. S. Wei and H. M. Xiong, *Nanoscale*, 2014, **6**, 13817-13823.
37 Y.-Q. Zhang, D.-K. Ma, Y. Zhuang, X. Zhang, W. Chen, L.-L. Hong, Q.-X. Yan, K. Yu and S.-M. Huang, *J. Mater. Chem.*, 2012, **22**, 16714-8.
38 S. Nigam, K. C. Barick and D. Bahadur, *J. Magn. Magn. Mater.*, 2011, **323**, 237-243.
39 C. Liu, P. Zhang, X. Zhai, F. Tian, W. Li, J. Yang, Y. Liu, H. Wang, W. Wang and W. Liu, *Biomaterials*, 2012, **33**, 3604-3613.
40 Y. Xu, A. Karmakar, D. Wang, M. W. Mahmood, F. Watanabe, Y. Zhang, A. Fejleh, P. Fejleh, Z. Li and G. Kannarpady, *The J. Phys. Chem. C*, 2010, **114**, 5020-5026.
41 S. A. Corr, Y. P. Rakovich and Y. K. Gun'ko, *Nanoscale Res. Lett.*, 2008, **3**, 87-104.

Dalton Transactions Accepted Manuscript

One-pot Synthesis Polyamines Improved Magnetism and Fluorescence Fe_3O_4-Carbon Dots Hybrid NPs for Dual Modal Imaging

Bo Li,[a,b] Xudong Wang,[a] Yali Guo,[a] Anam Iqbal,[a] Yaping Dong,[b] Wu Li,[b] Weisheng Liu[a] ,Wenwu Qin [a] [1], Shizhen Chen[c], Xin Zhou[c], Yunhuang Yang[c] *

Magnetic–fluorescent Fe_3O_4-CDs with dual modal imaging ability for both MRI and fluorescent imaging are prepared through one-step hydrothermal method.

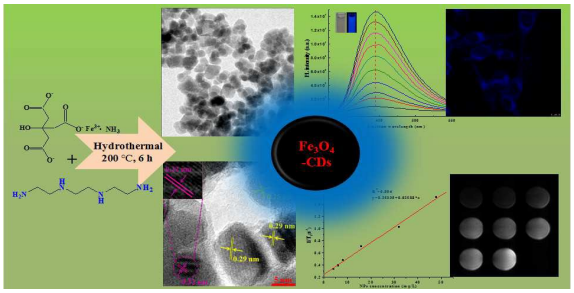

[1] Corresponding author: Fax: +86-931-8912582 E-mail address: qinww@lzu.edu.cn (W. Qin)； yang_yh@wipm.ac.cn (Y. Yang);

Dalton Transactions Accepted Manuscript